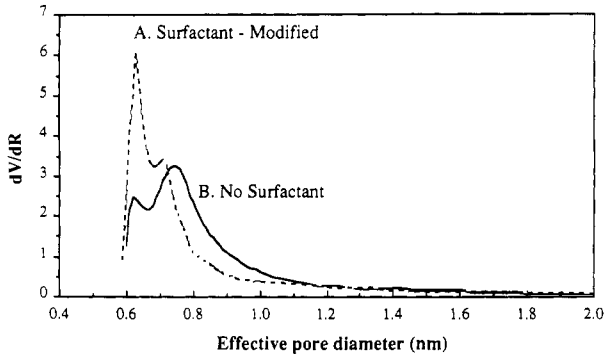

Figure 6. Micropore size distribution for calcined (500 °C, 19 h) alumina-pillared montmorillonites as determined by fitting the argon adsorption isotherm at −196 °C to the Horvath and Kawazoe model: (A) product obtained by $C_{12-14}E_5$ surfactant modification; (B) product prepared by conventional synthesis.

Table III. Comparison of Surface Areas and Pore Volumes Obtained from the Nitrogen and Argon Adsorption Isotherms for Calcined (500 °C) Alumina Pillared Clays[a]

	N_2 adsorption		Ar adsorption		
synthesis method	S_{BET}, m^2/g	V_m, cm^3 STP/g	S_{BET}, m^2/g	V_m, cm^3 STP/g	$[V_{liqN_2}/V_{liqAr}]$[b]
surfactant-modified	305	63.8	302	81.3	1.06
no surfactant	279	69.8	270	72.8	1.08

[a] Total surface areas (S_{BET}) and monolayer volumes (V_m) were obtained from a fit of the adsorption data to the BET equation. [b] Ratio of liquid monolayer pore volumes obtained by nitrogen and argon adsorption.

maximum is not understood at this time, but it may reflect the variation in layer charge distribution of the host clay.

A bimodal pore distribution also is observed for the pillared montmorillonite product prepared by conventional synthesis in the absence of surfactant. However, in this case the pore distribution occurs over a much broader range, from 0.6 to 1.1 nm. Also, much of the micropore structure found near 0.65 nm for the surfactant-modified clay has been replaced by a much broader pore distribution centered near 0.8 nm and extending beyond 1.1 nm in diameter. Thus, the surfactant-modified synthesis affords a pillared product with greatly improved pore size fidelity. The enhanced pore regularity might be facilitated in part by surfactant inhibition of Al_{13} hydrolyses prior to calcination to the final alumina-pillared product. Further studies are needed to test this hypothesis.

We also note from the results in Table III that the surface areas and microporous volumes obtained by argon and nitrogen adsorption are similar for the two adsorbates. In the case of a regularly microporous material, the ratio V_{mN_2}/V_{mAr} should be equal to 1, according to Gurvitsh's rule.[27] The ratio is somewhat closer to one for the clay prepared by surfactant modification, which is consistent with the more regularly microporous character of this material.

In a recent study related to our results for surfactant-modified pillared clay synthesis, Suzuki et al.[28] found that the addition of poly(vinyl alcohol) (PVA) to Al_{13} pillaring solutions increases the gallery height of alumina pillared fluorohectorite. In contrast to our $C_{12-14}E_5$ polyether surfactant, which causes immediate layer flocculation during Al_{13} exchange and does not alter the loading of Al_{13} oligomers in the galleries, PVA leaves the gallery space expanded and provides conditions for condensation of smaller Al oligomers into larger species. By controlling the gallery loading of aluminum, they were able to vary the gallery height of the alumina pillared clay over the range 9–19 Å. Whether the expanded galleries of PVA-modified pillared clay remained pillared or "stuffed" cannot be decided in the absence of surface area and pore volume data. The important point, however, is that $C_{12-14}E_5$ and PVA affect the gallery arrangement of Al_{13} oligomers in complementary ways and this adds diversity to strategies for manipulating the pore structure of pillared clays.

Acknowledgment. The support of this research under NIEHS Grant ESO-4911B is gratefully acknowledged.

(27) Gregg, S. J.; Sing, K. S. W. *Adsorption, Surface Area and Porosity*, 2nd ed.; Academic Press: London, 1982; p 113.
(28) Suzuki, K.; Masakazee, H.; Masuda, H.; Mori, T. *J. Chem. Soc., Chem. Commun.* **1991**, 873.

Structural Features of Sol–Gel-Derived Hybrid Inorganic–Organic Network Ceramer Materials by Small-Angle X-ray Scattering

D. E. Rodrigues, A. B. Brennan, C. Betrabet, B. Wang, and G. L. Wilkes*

Department of Chemical Engineering, Virginia Polytechnic Institute & State University, Blacksburg, Virginia 24061

Received May 5, 1992. Revised Manuscript Received September 21, 1992

Hybrid inorganic–organic materials called ceramers have been prepared in our laboratories utilizing the sol–gel approach. These materials have been previously characterized, and a general morphological mode has been proposed based primarily on the small-angle X-ray scattering (SAXS) data. This paper focuses on the morphological model and tests its validity (using SAXS) under a variety of variables such as temperature, metal alkoxide content, oligomer spacer length, effect of different solvents, etc. The last part of this paper further addresses the nature of the inorganic particles formed in these systems and discusses their physical features based on fractal concepts.

Introduction

In recent years the sol–gel process has been utilized in our laboratories to react metal alkoxides such as titanium(IV) isopropoxide, zirconium *n*-propoxide, aluminum *sec*-butoxide, and tetraethylorthosilicate with oligomers such as poly(tetramethylene oxide), polyimide, poly(ether ketone), and polysulfone end-capped with silicon alkoxide functionalities to yield hybrid inorganic–organic network

* To whom correspondence should be addressed.

0897-4756/92/2804-1437$03.00/0

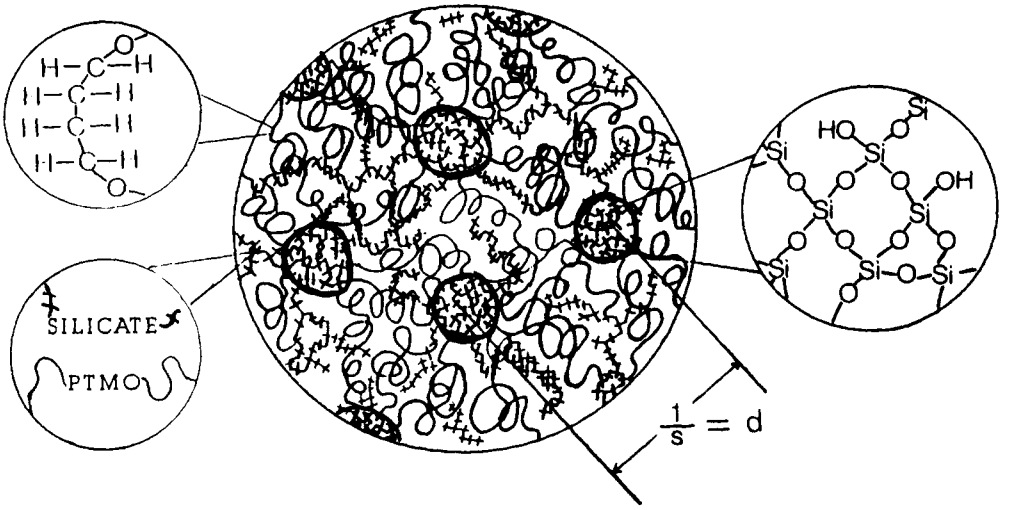

Figure 1. General morphological model for metal alkoxide/PTMO ceramers. The average interdomain spacing as measured by SAXS is indicated by the letter *d*. The regime in the upper left circle represents the organic oligomeric rich regimes, while the lower left circle represents the regions in which the two components (organic and inorganic) are mixed. The regime on the right represents the inorganic rich regions.

materials termed "ceramers".[1-4] Depending upon the choice of metal alkoxide and oligomer and the respective composition ratio of the two, the resulting film can be flexible or stiff and monolithic and display several properties which are intermediate between those of the oligomeric and the inorganic components. The cast films obtained are optically transparent. Such a materials chemistry approach can therefore be used to produce a multitude of systems with widely varying properties which depend upon the type of metal alkoxide as well as the oligomer chosen. Several other parameters such as catalyst content (acid or base), solvent, amount of water (during the sol–gel reaction) and reaction temperature, etc., have also been found to affect the general structure–property behavior of these materials. However, a more complete description of the synthetic aspects of these materials lies beyond the general objectives of this paper, and the reader is referred to a recent review which describes the general features of these ceramers in more detail.[5]

As stated above, these ceramer films have been found to be transparent, which is an indication of a lack of macrophase separation. However, on a microscopic level ca. 10 nm, compositional differences appear as suggested from small-angle X-ray scattering (SAXS).[6-9] The SAXS profiles provide information on any systematic fluctuations in the average electron density of a scattering source when the scale length over which such fluctuations occur is ca. 5–100 nm. These concentration fluctuations in the ceramer films are dependent upon the compatibility of the oligomeric and inorganic components which in turn influences the nature of growth of the inorganic phase. On the basis of previous experimental evidence, a general morphological model was proposed for this microphase behavior and is shown in Figure 1. The model displays three generalized regimes or phases which make up the ceramer morphology. The first regime identified in the upper left circle represents the organic oligomeric-rich regimes. The regime in the lower left-hand circle indicates the regions in which the two components (organic and inorganic) are mixed, while the circle on the right-hand side represents the inorganic-rich regions. An estimate of the spacing between the inorganic rich regions as measured using SAXS is represented by the average interdomain spacing *d*. While this model has been described in some detail elsewhere[5] for some specific materials, no attempt has been made thus far to systematically address the various morphological changes expected in these hybrid networks with a variety of changes in the molecular variables. This is the objective of this paper.

The model, thus described above, suggests the separation of a dispersed inorganic-rich phase chemically crosslinked at the interface with an oligomeric-rich matrix phase leading to the development of an interdomain spacing as can be measured from an interference peak in the SAXS profile. It should be noted that all metal alkoxides undergo a reduction in volume when the hydrolysis and condensation reactions take place, and as a result of this behavior the oligomeric phase in the ceramer systems will in general form the matrix except at very high *initial weight* composition ratios of metal alkoxide/oligomer such as the case of the ceramer containing 80 wt % metal alkoxide as described in section f of this paper. This ratio will vary from system to system depending upon the nature of growth of the inorganic phase. The interdomain spacing as well as the intensity of scattering has been found to be dependent upon several parameters such as the nature of the metal alkoxide, metal alkoxide content, temperature of processing, etc. It was therefore decided to test the validity of this general model by using SAXS to study changes in the morphological features as a function of some of these reaction or composition parameters. The purpose of this paper is to systematically address some of the structural features of these ceramer films (determined from SAXS measurements) as a function of (a) type of metal alkoxide, (b) temperature of cure, (c) metal alkoxide content, (d) oligomer molecular weight, and (e) swelling of the final network.

Of additional importance is to recognize that when metal alkoxides such as tetraethylorthosilicate (TEOS) and zirconium *n*-propoxide are reacted via the sol–gel technique

(1) Huang, H.; Orler, B.; Wilkes, G. L. *Polym. Bull.* **1985**, *14*, 557.
(2) Huang, H.; Orler, B.; Wilkes, G. L. *Macromolecules* **1987**, *20*, 1322.
(3) Wang, B.; Brennan, A. B.; Huang, H.; Wilkes, G. L. *J. Macromol. Sci., Chem.* **1990**, *A27*, 1449.
(4) Huang, H.; Glaser, R. H.; Wilkes, G. L. *ACS Symp. Ser.* **1987**, *360*, 354.
(5) Wilkes, G. L.; Brennan, A. B.; Huang, H. H.; Rodrigues, D. E.; Wang, B. *Mater. Res. Soc. Symp. Proc.* **1990**, *15*, 171.
(6) Brennan, A. B.; Rodrigues, D. E.; Wang, B.; Wilkes, G. L. *J. Inorg. Organomet. Polym.* **1981**, *167*, 1.
(7) Huang, H.; Wilkes, G. L.; Carlson, J. G. *Polymer* **1989**, *30*, 2001.
(8) Noell, J. L. W.; Wilkes, G. L.; Mohanty, D. K.; McGrath, J. E. *J. Appl. Polym. Sci.* **1990**, *40*, 1177.
(9) Rodrigues, D. E.; Wilkes, G. L. *ACS Prepr.* **1989**, *30*, 227.

(no functionalized organic present), the resultant metal oxide particles display fractal behavior, i.e., they display dilational symmetry or self-similarity at different levels of magnification. The details of the fractal analysis on such silicate particles (developed from acid- and base-catalyzed TEOS) from SAXS data have been provided by Brinker et al.,[10] Keefer[11] and Schaefer.[12,13] In the context of fractal behavior displayed by such silicate particles, Schaefer et al. have stated that the acid-catalyzed systems display mass fractal behavior while species produced in a base-catalyzed reaction of TEOS are generally more colloidal and display surface fractal behavior. Fractal dimensions can be obtained from the slope in the Porod region of the SAXS profiles when the data are plotted in the form of log $I(s)$ vs log s, s being defined as $(2/\lambda) \sin \theta$, where θ is one-half of the radial scattering angle and λ is the wavelength. Another angular variable commonly used is that of q or κ, both of which are equal to $2\pi s$. Mass fractals have the property that the mass M varies as a power of the characteristic length or size, i.e., $M \propto (\text{length})^D$, D being the fractal dimension. Mass fractal dimensions are always less than the dimension of the space in which the fractal exists, which implies that the mass of the particulate increases less rapidly than the volume it occupies.[11,12] For mass fractals the Porod slope, x, is related to D as $x = -D$. For mass fractal structures $-1 \leq x \leq -3$ when the incident beam is of point or pinhole geometry, while for slit-smeared intensity, $0 \leq x \leq -2$ because of the smearing effect.[12] Fractal surfaces, on the other hand, have the property that the surface area S varies as a noninteger power of the length $S \propto (\text{length})^{D_s}$, D_s being the surface fractal dimension. Fractal surfaces are characterized by a Porod slope $x = D_s - 6$. Thus for surface fractals, $-3 \leq x \leq -4$ for pinhole collimation (point source) while after correction for slit smearing $-2 \leq x \leq -3$. In other words D_s is a measure of surface roughness of the scattering particle. It should be noted that since all the data presented in this paper were obtained in the infinite-slit configuration, the slopes reported have been corrected to that which would be obtained from a point source by adding a factor of -1 to each slope. As shown by Keefer and Schaefer, both types of fractal structures (mass and surface) are possible for silicate sol–gel materials. To study the development and structure of the inorganic phase in these ceramer systems, SAXS measurements were also made on two selected ceramer materials as the network reaction proceeded following gelation. These results were then analyzed to determine the fractal dimensions as well as the radius of gyration of the dispersed inorganic particles. Some preliminary results of this work will also be provided in this paper due to its relevance to the general morphological model.

Experimental Section

The general nomenclature for these ceramers has been previously described[1] and will be summarized very briefly here. As an example, a material indicated by TiOPr(50)-PTMO(2K)-25-0.06 contains 50 wt % of titanium(IV) isopropoxide with respect to the sum of the weights of TiOPr and (isocyanatopropyl)triethoxysilane end-capped polytetramethylene (PTMO) of number-average molecular weight 2000 g/mol. Water in a stoichiometric amount equivalent to 25% (mol/mol) of the total quantity necessary to hydrolyze all the alkoxy functionalities present in the reaction mixture was added along with 0.06 (mol/mol) of the catalyst HCl. The same nomenclature has been applied to the zirconium isopropoxide (ZrOPr)/PTMO, tetraethylorthosilicate (TEOS)/PTMO, and TiOPr/polyimide ceramers described in this paper as well. Unless otherwise stated isopropyl alcohol was used for compatibilizing the reactants before the addition of catalyst. Details for the preparation of all of these materials have been provided elsewhere.[1-7]

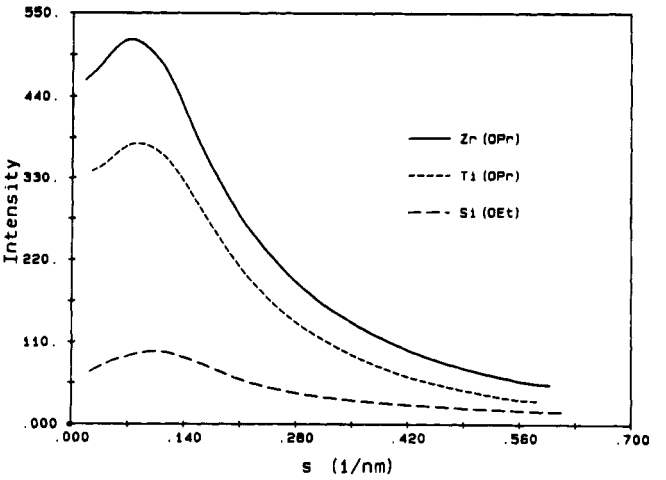

Figure 2. SAXS behavior of ceramer compositions TEOS-(50)-PTMO(2K)-100-0.048, TiOPr(50)-PTMO(2K)-25-0.06, and ZrOPr(50)-PTMO(2K)-0-0.06.

SAXS was performed on all samples using Cu Kα radiation with a wavelength of 1.54 Å. The SAXS facility utilized a Kratky-Siemens camera and a Braun position-sensitive detector. All data are slit smeared with the entrance slit width being 100 μm. The SAXS profiles are displayed on a plot of intensity $I(s)$ versus the scattering vector s. The intensity $I(s)$ is the absolute intensity and has been normalized by sample thickness. The characteristic average d spacing or interdomain spacing for these materials can be estimated from the reciprocal of the scattering vector s for the interference peak position in the SAXS profile. All the scattering data profiles displayed in this paper were treated to remove parasitic scattering. The scattering profiles have not, however, been treated to remove thermal density fluctuations which typically exist in two-phase systems. While it is realized that these fluctuations slightly raise the intensity of the scattering profile in the systems at hand, the degree of scattering is quite strong due to the differences in electron density of the metal oxide species relative to the organic component and thus such fluctuations should be of lesser importance. Since no fully accepted theory exists to easily remove this background component, we therefore have neglected this correction which we believe will be small in most of the systems discussed in this paper. We do caution the reader, however, that while the concepts developed here are believed to be sound, the degree of quantitative accuracy may be less due to the neglection of such thermal density fluctuations. It should also be noted that the use of slit smeared data causes any measured interdomain spacing from an interference peak to increase (i.e., the peak actually occurs at smaller angles when a point source is utilized). Hence desmearing would be required in order to obtain a more accurate estimate of the d spacing. However, the use of smeared data will not influence our conclusions.

Results and Discussion

(a) Effect of the Type of Metal Alkoxide on the SAXS Peak Position and Intensity. Here the metal alkoxide composition (before reaction) was maintained at 50 wt % with respect to the sum of the weights of metal

(10) Brinker, C. J.; Keefer, K. D.; Schaefer, D. W.; Assink, R. A.; Kay, C. D.; Ashley, C. S. *J. Non-Cryst. Solids* **1984**, *63*, 45.
(11) Keefer, K. D. Better Ceramics Through Chemistry II. *Mater. Res. Soc. Symp. Proc.* **1986**, *121*, 295.
(12) Schaefer, D. W.; Keefer, K. D. *Phys. Rev. Lett.* **1984**, *53*, 1383.
(13) Schaefer, D. W.; Keefer, K. D. Better Ceramics Through Chemistry II. *Mater. Res. Soc. Symp. Proc.* **1986**, *73*, 277.
(14) Brinker, C. J.; Scherer, G. W. *Sol Gel Science*; Academic Press: San Diego, CA, 1990.
(15) Keefer, K. D. *Silicon Based Polymer Science*; Zeigler, J. M., Gordon Fearon, F. W., Eds.; ACS Advances in Chemistry Series; American Chemical Socity: Washington, DC, 1990; p 224.

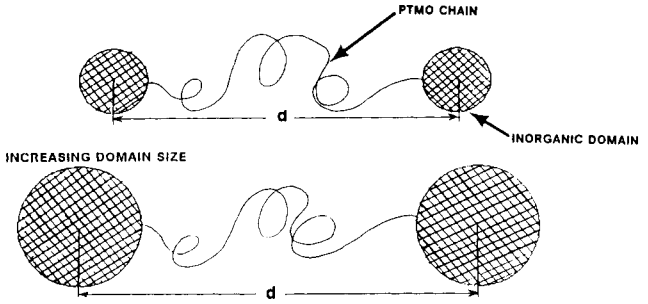

Figure 3. Schematic shows the effect of increasing inorganic domain size on the interdomain spacing as measured from SAXS.

alkoxide and functionalized PTMO, but the metal alkoxide was varied from TEOS to TiOPr to ZrOPr. The method of preparation of these ceramers has been previously described by Wang.[3] As can be seen from Figure 2, all the three ceramers display very similar SAXS profiles each of which show a single interference peak suggesting the existance of a microphase-separated morphology. The scattering intensity is lowest for the ceramer containing TEOS and is highest of for the ceramer containing ZrOPr. This increase in the scattering intensity is expected if relatively comparable morphologies are generated due to the increase in the scattering power of the inorganic phase. That is, as the atomic number of the inorganic component increases, so does the mean-square electron density difference between the inorganic and the oligomeric components which in turn causes an increase in the scattering intensity. Since the atomic number of Zr > Ti > Si the scattering power also decreases in the same order and hence the ZrOPr/PTMO ceramers show the highest scattering intensity while those constituted of TEOS/PTMO show the lowest. The similarity in the scattering profiles would indicate that the general morphology as shown in the model in Figure 1 is similar for these three ceramer systems although some difference in the peak position does occur.

It is also evident from the scattering profiles in Figure 2 that the intensity maxima in the scattering profiles shifts toward smaller s values (larger interdomain spacings) as the metal alkoxide is changed from TEOS to TiOPr to ZrOPr. Since the weight fraction of metal alkoxide is constant and the molecular weight of the oligomer "spacer" is fixed at 2000 g/mol, this result suggests that the size of the scattering domains may be dependent upon the reactivity of the respective metal alkoxides. Both ZrOPr and TiOPr are known to be more reactive than TEOS and these faster reacting metal alkoxides are known to self-condense and precipitate from their respective sols. Brennan et al.[6] has suggested that the reason for this systematic increase may be due to the fact that the reactivity of ZrOPr > TiOPr > TEOS. Another possible explanation for this observed effect is the fact that TiOPr and ZrOPr (but not TEOS) are prehydrolyzed prior to adding the functionalized PTMO. This may lead to the formation of particulates somewhat larger in size than those formed in the TEOS-based ceramers, where the growth of the silicate particles may be restricted because of the PTMO network. The inorganic domains formed in the ZrOPr/PTMO system may be speculated to be larger than those in the TiOPr/PTMO system which in turn are larger than those in the TEOS/PTMO ceramer system. This feature is displayed clearly in Figure 3, where the increase in the size of the scattering particles at the oligomer chain ends promotes an increase in the interdomain spacing. It should be noted that the diagram in Figure 3 is not an actual representation of the morphology of the system but rather a sketch to enable the reader to better comprehend the behavior of the system. Finally, the above explanation of the observed SAXS behavior presumes that the scattering is of interparticle origin in contrast to intraparticle. Further support for this argument will be provided later in this paper.

(b) Effect of Cure Temperature on the Scattering Profiles. In this experiment TiOPr (18 wt %) was reacted with a particular 6F-based polyimide of molecular weight 8400 g/mol. The solvent used for compatibilization of these two reactive components was *N*-methylpyrrolidone. The method of preparation of this functionalized polyimide oligomer is shown in Figure 4. The structure of the ceramer film was then evaluated as a function of annealing (curing) temperature using SAXS. All the SAXS profiles, however, were conducted at room temperature. The sample was prepared by solution casting at room temperature. It was then heated to 60 °C for 3 days to gel, followed by a cure at 100 °C for an additional 3 days. This was followed by a slow heat to 150 °C, where it was held for 20 min. The sample was then analyzed by SAXS under ambient conditions and then annealed to 270 °C for 20 min. The SAXS behavior was again determined. The final thermal treatment was at 325 °C for 20 min again followed by SAXS analysis. The SAXS profiles for the sample thermally treated to the three different temperatures can be seen in Figure 5. The intensity at the peak position

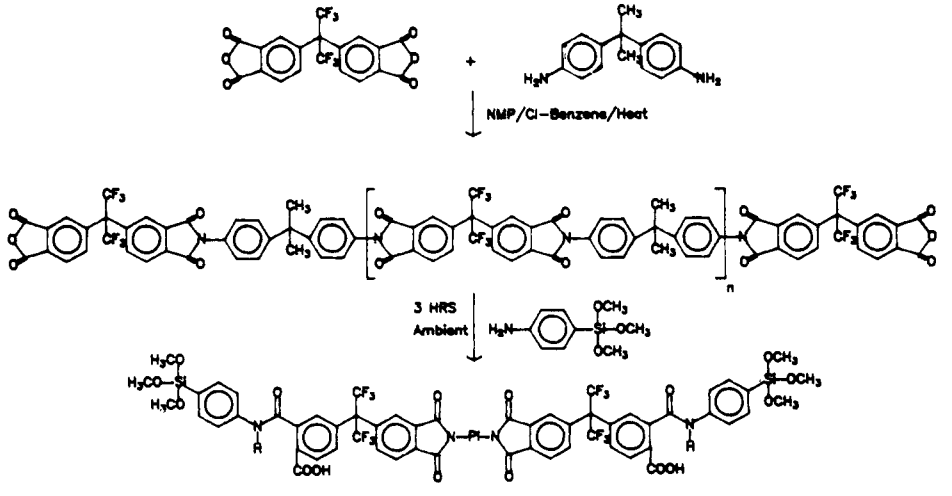

Figure 4. Reaction scheme for end-functionalized 6-fluorobenzophenonetetracarboxylic acid dianhydride/bisaniline (6F-BTDA/Bis A) polyimides.

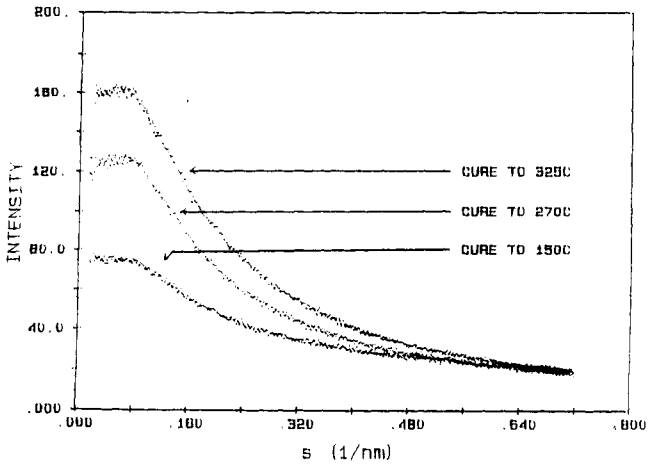

Figure 5. SAXS profiles for a TiOPr/polyimide ceramer cured stepwise to three different temperatures.

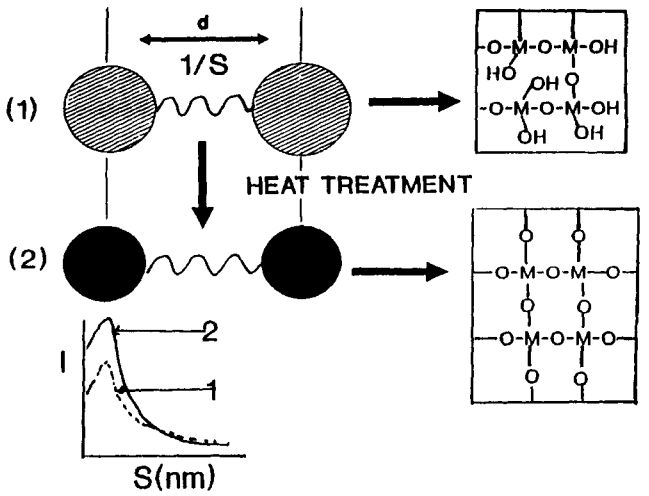

Figure 6. Schematic illustrates the effect of heat treatment on the inorganic domains and the interdomain spacings as measured from SAXS.

can be seen to systematically increase with temperature though the "smeared" interdomain spacing or characteristic length remains essentially the same at ca. 15 nm. As schematically shown in Figure 6, the increase in the maximum intensity with annealing temperature is strongly believed to be due to densification in the inorganic domains which promotes an increase in the mean-square electron density fluctuation. Increased densification in the inorganic domains would also suggest a greater extent of reaction within the system. The lack of any *major* change in the interdomain spacing indicates that the general microphase morphology remains the same despite the densification of the inorganic domains as would be expected based on the general model. There may be some questions as to whether such a densification process would also promote an increase in the end-to-end distance of those oligomer chains which are connected to the surface or core of an inorganic particle due to the densification process as shown in Figure 6. However, further experimentation needs to be conducted on these materials to determine this effect possibly by use of deuterium-labeling techniques and small-angle neutron scattering. It should be stated that many similar observations of the effect of curing temperature on the SAXS behavior of other related ceramers have also been noted in our overall studies.[5] Some examples include oligomers based on poly(ether ketone), poly(arylene ether sulfone), and poly(ether phosphine oxide).

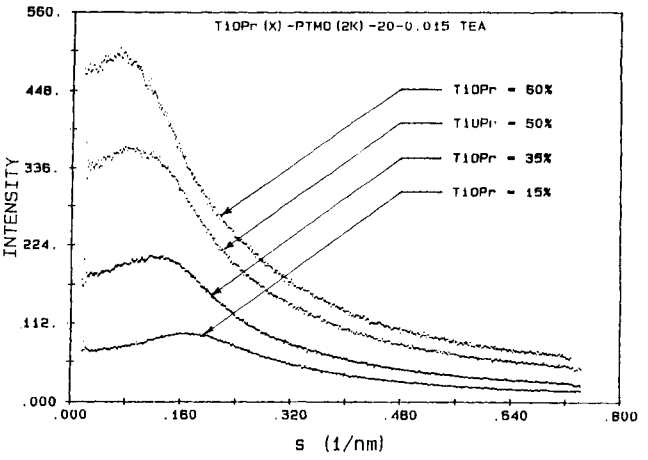

Figure 7. SAXS profiles for TiOPr/PTMO films containing varying amounts of TiOPr.

(c) Effect of Metal Alkoxide Composition of the Scattering Intensity and the Interdomain Spacing. In this experiment the composition of TiOPr was varied from 15 to 60 wt % (with respect to the combined weight of the end-capped PTMO and the metal alkoxide) but the molecular weight of the PTMO (organic matrix spacer prior to endcapping) was maintained constant at 2000 g/mol. Water was used for hydration of the alkoxy functionalities in a 25% (mol/mol) ratio and 0.015 (mol/mol) of triethylamine catalyst was added to the reaction mixture. The triethylamine catalyst is more alkaline in nature, and its use in this experiment was initially undertaken to determine the difference in ceramer microstructure when base catalysis was used versus acid (HCl) catalysis. From these studies it was discovered that the nature of the catalyst does not greatly affect the final structure of the ceramer, and this is believed to be partially due to the high reaction rate of TiOPr which renders the catalyst less influential on the structure of the final product.

The SAXS results for the variation of the TiOPr content in this series of TiOPr/PTMO ceramers can be seen in Figure 7. All the scattering profiles in the figure display a single interference peak which, as stated earlier, is indicative of a non-highly periodic fluctuation of the electron density within the films. The maximum scattering intensity as well as the interdomain spacing (as estimated from the reciprocal of the scattering vector s) can be seen to increase with an increase in metal alkoxide content. The interdomain spacing increases from ca. 70 to 170 Å as the weight fraction of TiOPr is increased from 15% to 60% as shown in Figure 8. Our morphological model would predict an increase in the interdomain spacing primarily due to the greater size of the scattering particles (as in Figure 3) as metal alkoxide content in the ceramer increases so long as the oligomer molecular weight or the "organic matrix spacer" is kept constant and that either the bonding of the terminal points of the oligomer chains occurs primarily at the surface regions of the inorganic phases. In Figure 8 it can be seen that when the TiOPr content decreases to zero, the value of d becomes close to that expected for the root-mean-square (RMS) end-to-end distance calculation for a 2000 g/mol PTMO chain (assuming Gaussian statistics) which is approximately 43 Å; this is indicated by an arrow in the figure. The network formed at zero TiOPr content results from the reaction of the triethoxysilane end-capped PTMO. In fact the interdomain spacing as measured from SAXS would further decrease to the calculated RMS end-to-end distance for the oligomer if the scattering data were desmeared. This

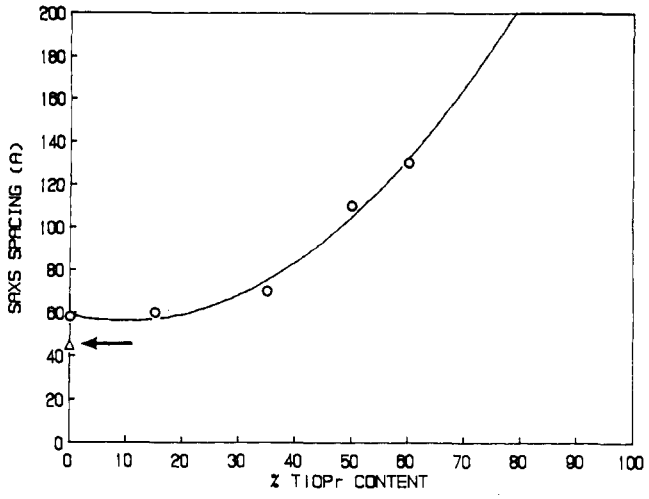

Figure 8. Plot showing increased interdomain spacing as the metal alkoxide content in the TiOPr/PTMO ceramer materials is increased. The arrow on the left indicates the end to end distance for a 2000 g/mol PTMO chain as calculated from Gaussian statistics.

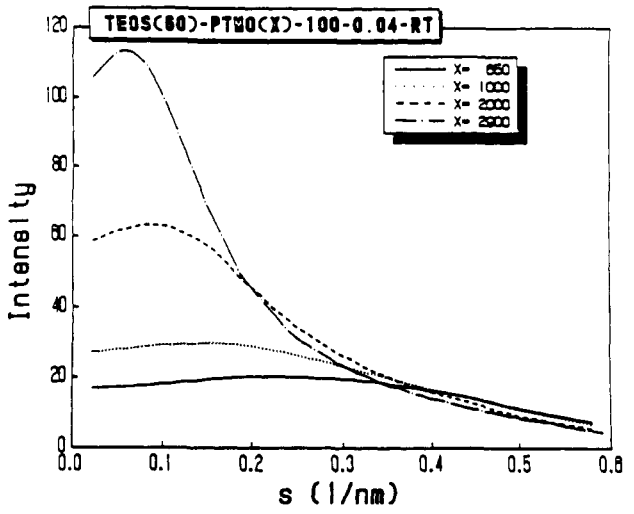

Figure 9. SAXS profiles of materials prepared with 60 wt % TEOS and various molecular weights of end-functionalized PTMO.

lends further credence to the general model, i.e., the interference peak is due to interparticle scattering rather than due to intraparticle scattering. There may, however, be some contribution from intraparticle scattering at the *higher angles* due to porosity (density fluctuations) within the inorganic phase in some of these ceramer systems.[16] It might also be restated that there is some concern as to whether or not partial oligomer chain extension occurs in the final structure with increasing metal alkoxide content in the ceramer system. However this concern has neither been proven nor disproven but could be best investigated by use of SANS of labeled PTMO chains as mentioned earlier.

(d) Effect of Oligomer Molecular Weight on the Peak Position. To further verify whether the peak seen in the SAXS spectra is caused by the average distance between domains (interparticle scattering), the molecular weight of the pre-end-capped PTMO was varied from 650 to 2900 g/mol. That is, the organic molecular spacer was increased in length which in turn should increase the characteristic d spacing. TEOS was added at 50 wt % as the inorganic component. Water was added in a 100% (mol/mol) ratio, while acid catalyst was added to the reaction mixture in a 0.048 (mol/mol) ratio to the reaction mixture. The method of preparation of these ceramers has previously been described by Huang.[1]

As can be seen in Figure 9 these scattering profiles each show a broad maxima which increases in intensity with increasing molecular weight of the oligomer. This result confirms that the peak is due to interparticle scattering interference because as the molecular weight of the oligomer increases, the end-to-end distance of the PTMO chain increases. This increase in the end-to-end distance of the PTMO chains would cause the inorganic domains to be spaced further apart from each other as inferred from the SAXS results. It is also noted that the overall integrated intensity decreases as the molecular weight of the spacer decreases from 2900 to 650 g/mol. This result clearly suggests differences in the level of mixing that occurs between the two components if it is assumed that the extents of reaction for each member of the series is equivalent. In other words, since the basic composition ratio of the inorganic alkoxide to the functionalized oligomer is constant throughout the series, it might be expected that the invariant of the respective SAXS profiles would be identical. The invariant for a sharp two-phase system reflects the mean-square fluctuation in electron density $\langle \rho^2 \rangle$ where the latter is given by

$$\langle \rho^2 \rangle = \phi_1 \phi_2 (\rho_1 - \rho_2)^2 \quad (1)$$

where ϕ_1 and ϕ_2 are the volume fractions of the two phases respectively and ρ_1 and ρ_2 are their respective electron densities. Clearly, from direct inspection of the smeared SAXS profiles, it is obvious that the integrated intensity will not be constant and decreases as the molecular weight decreases. This can be easily explained if there is some level of increased mixing of the inorganic and the oligomeric components as the molecular weight of the latter decreases. The fact that there is a broader less defined interference peak with lower PTMO molecular weight strongly implies that this hypothesis is a reasonably one to account for the decreased overall scattering intensity.

Huang[1,2,4] performed dynamic mechanical analysis on this same series of films and from the tan δ results concluded that the ceramer containing the lowest molecular weight oligomer possessed little polymer-rich material. This increase in the temperature for the onset of cooperative segmental motion could be due to additional restrictions brought on by crosslinking of the PTMO. The intensity of relaxation due to the existence of a polymer-rich phase was found to gradually increase with the molecular weight of the oligomer. These results correlate very well with the SAXS analysis.

(e) Effect of Swelling. To make an additional verification of the fact that the scattering peak is due to interparticle interference, a TiOPr(20)-PTMO(2K)-25-0.06 ceramer sample was subjected to swelling in tetrahydrofuran (THF) for 1 day, and the scattering profile was measured before and after the swelling experiment. From Figure 10 the interdomain spacing increases from 97 to 110 Å due to 15 wt % swelling. Though the peaks in the scattering profiles of Figure 10 are not easy to visualize, the interdomain spacings are measured at the position of maximum intensity. The intensity of scattering also drops slightly, and this is attributable to a decrease in the volume fraction of the inorganic phase due to solvent uptake in the swollen film. It is expected that the solvent is preferentially absorbed by the PTMO-rich regions. The increase in the interdomain spacing is analogous to increasing

(16) Rodrigues, D. E.; Wilkes, G. L., manuscript in preparation.

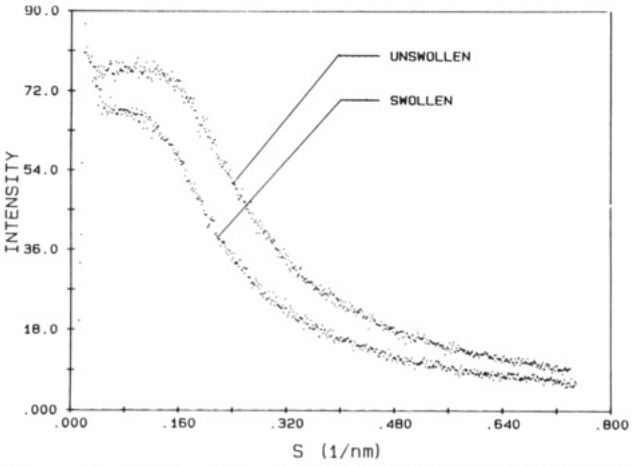

Figure 10. SAXS profiles of a TEOS(20)-PTMO(2K)-100-0.048 ceramer before and after swelling in THF.

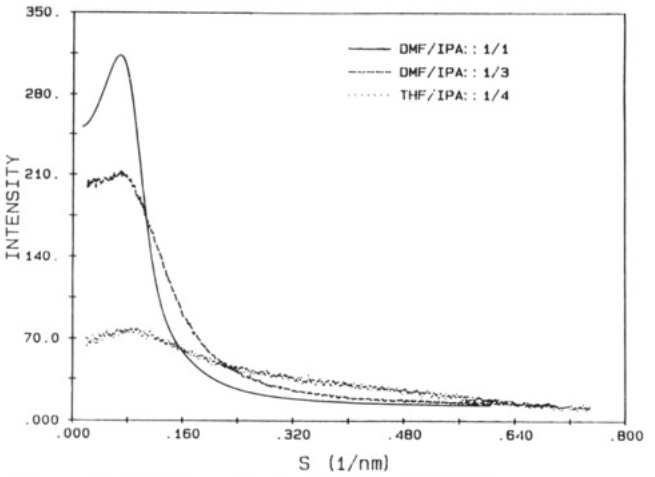

Figure 11. SAXS profiles for TEOS(60)-PTMO(2K)-100-0.048 ceramers as a function of different reaction media.

the length of the oligomeric spacer connecting the inorganic domains.

(f) Effect of Solvent Type on the Structure of the Cast Ceramer. This experiment was conducted to study the effect of different solvents on the nature of the inorganic phase. The material used for this study was TEOS(60)-PTMO(2K)-100-0.048, and the TEOS/PTMO reactants were reacted in either IPA or a cosolvent system of *N*,*N*-dimethylformamide (DMF) and IPA in a volume ratio of 1:3 or 1:1. The scattering profiles shown in Figure 11 are those obtained for these three ceramers cast under identical conditions. It can be seen that as the DMF content in the ceramers is increased, the scattering profile becomes much sharper. This indicates a narrower distribution of either domain sizes or interdomain spacings or both. This is believed to be attributable to the higher value of the pH of the mixture when DMF is used as cosolvent and which from previous studies has been found to promote less mixing between the inorganic and the oligomer in the ceramer.[9] As the peak sharpens, its scattering intensity increases and the intensity in the tail region decreases indicating once again that there is less mixing between the two phases. As the ratio of DMF to IPA is increased above unity, macrophase separation between the inorganic and the oligomer phase begins to occur as becomes obvious from the observance of high turbidity.

Since there is a high degree of phase separation between the metal oxide and the oligomer in the case of the TEOS/PTMO ceramers reacted in DMF/IPA, it was decided to vary the metal alkoxide composition (from 40 to

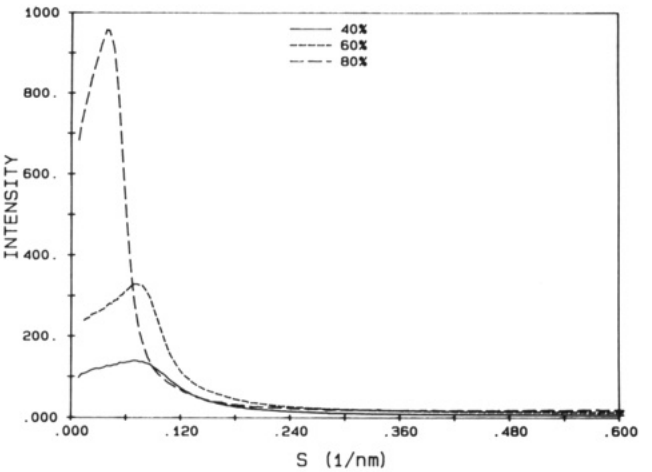

Figure 12. SAXS profiles for TEOS/PTMO ceramers reacted in DMF/IPA, where TEOS content is varied from 40 to 60 to 80 wt %.

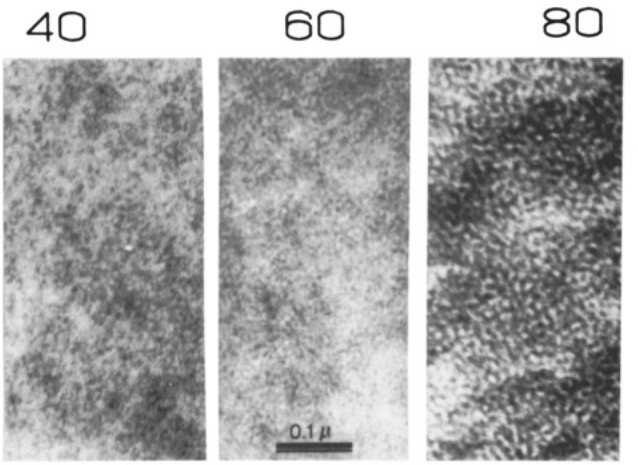

Figure 13. TEM micrographs of the TEOS/PTMO ceramers reacted in DMF/IPA, where TeOS content varied from 40 to 80 wt %.

60 to 80 wt %) with respect to the PTMO and perform transmission electron microscopy (TEM) on the resultant films in order to obtain an actual image of the microstructure of these materials. The SAXS profiles for these TEOS/PTMO materials is shown in Figure 12 where the TEOS composition is varied from 40 to 60 to 80 wt %. It can be seen that as the weight fraction of TEOS is increased, the intensity of scattering increases and the peak position shifts to smaller angles indicating an increase in the interdomain spacing as stated earlier. The TEM micrographs seen in Figure 13 show no particular long-range order in any of these materials. The approximate values of interdomain spacing as measured from these micrographs are similar to those measured from SAXS. For example, for the 80 wt % TEOS/PTMO sample the measured interdomain spacing from is 260 Å, while the measured value from the TEM micrograph averages around 210 Å. In these micrographs the white phase represents the PTMO, while the more electron-dense silicate phase appears dark. As the TEOS content is increased, there appears to be an increase in the particle size as seen from the micrograph. This was earlier proposed in the general morphological model for these ceramers. In the micrograph it can be seen that the darker regions for the TEOS(60)-PTMO(2K)-100-0.048 film are better defined than those in the TEOS(40)-PTMO(2K)-100-0.048 material, and this indicates that there is greater phase separation between the metal oxide and oligomeric phases

as the metal alkoxide content in this ceramer is increased. This will be alluded to further in an upcoming paper. The 80 wt % TEOS/PTMO ceramer shows an even greater distinction between the dark and white phases suggesting an even greater degree of phase separation. However, for this material (80 wt %) it can be seen that there is connectivity between the inorganic phases indicating that there may be impingement of the inorganic domains at this high metal alkoxide composition.

Clearly the general features of the morphological model seem well justified, but the details of the structural features of the inorganic phase are not really addressed, i.e., is the phase particulate smooth or open and rough, or of fractal character? The next section will briefly probe these questions.

Study of Inorganic Particulate Structure from Fractal Analysis

From the studies conducted to verify the general morphological model, it has been demonstrated that these ceramers typically display some level of microphase separation, and the scattering particles display correlated behavior on a distance scale that is of the order of 100 Å. However, as stated above, the characteristics of these dispersed inorganic phases has not yet been addressed. Therefore, to study the nature and characteristics of the dispersed phase as well as the phase separation in these ceramer systems, it was decided to attempt to estimate the radius of gyration and their potential fractal dimensions from the SAXS behavior. The ceramer composition selected for this experiment was TEOS(60)-PTMO(2K)-100-0.048. The reason for the use of TEOS as the inorganic precursor (and not TiOPr or ZrOPr) stems primarily from the fact that the scattering behavior for the TEOS-based ceramers is dependent upon the solvents used to compatibilize the reactants, while no such dependency is seen for the TiOPr- and ZrOPr-based systems. The reactivity of the TiOPr and ZrOPr is much greater than the TEOS and the structure of the resulting inorganic has been found to be independent of the choice of catalyst (either acidic or basic). Silicate structures, however, are dependent upon whether the TEOS is acid catalyzed or base catalyzed. The reactants, i.e., TEOS and PTMO, were first compatibilized in either a 1:4 volume ratio of THF and IPA or a 1:1 volume mixture of DMF and IPA. To these mixtures were added the water and the HCl catalyst. The method of preparation of these ceramers has been described elsewhere.[9]

The use of DMF along with IPA in the preparation of these TEOS/PTMO ceramers has been previously shown (in section e above) to produce a sharper scattering peak than those seen in the other ceramer systems discussed above. This indicates a narrower distribution of domain spacings or domain sizes or both. This behavior is believed to be because of the pH of DMF, which is approximately 6.7, and this promotes a more particulate-like behavior in the silicate species than when THF/IPA is utilized as the compatibilizing solvent. When THF/IPA is used as the compatibilizing cosolvent the silicate species is more open or ramified.[9]

For these experiments the reactants were poured into a polystyrene Petri dish after the addition of the acid catalyst. The reactants cured at ambient conditions in DMF/IPA took 30 min to form a stable gel which did not flow and which was analyzed by SAXS at 30 min, 2 and 12 h, and 2 weeks after the addition of catalyst. The TEOS/PTMO reactants cured in THF/IPA took longer to gel, and the first scattering profiles were obtained at 6 h, followed by readings at 12 h and 2 weeks. The scattering

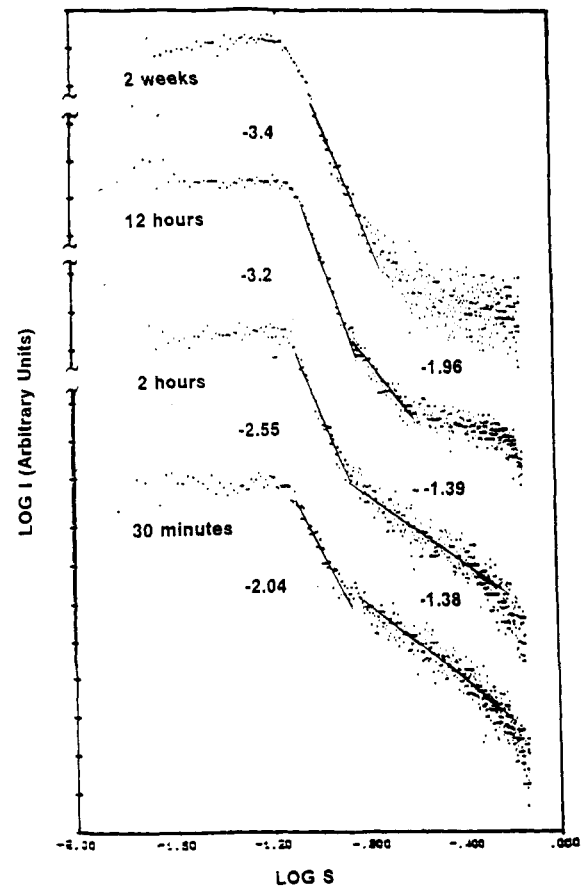

Figure 14. Fractal dimensions obtained (from slopes in the Porod region of the SAXS scattering curves) on a TEOS(60)-PTMO-(2K)-100-0.048 ceramer reacted in DMF/IPA during the gelation process.

experiments were performed on the gel in the polystyrene Petri dishes, and later the scattering due to the polystyrene was subtracted from the overall scattering profile. The corrected scattering profile was then analyzed in the Guinier region for the electronic radius of gyration of the inorganic particles and the Porod region for possible fractal behavior. It should be pointed out that the radius of gyration as well as the fractal dimensions were obtained from scattering data that contains a weak interference peak, and hence the quantitative results should again be considered only for the trends they provide and not for the absolute values. Similar analysis has been previously applied by Schaefer et al.[17] in pure sol–gel metal alkoxide systems to obtain fractal dimensions.

The analysis in the Porod region for the material reacted in DMF/IPA is shown in Figure 14. The scattering data have been plotted on a log–log scale and the profiles have been vertically shifted to avoid data overlap. It can be seen that after 30 min of the addition of acid the gel shows two distinct linear regions with "corrected" slopes as discussed earlier. The slope at smaller angles is more negative than −2 while the slope in the higher angular region is approximately −1.4. The slope of −2.0 indicates that these particles may initially be branched mass fractals.[11-13] Recall that mass fractal structures give slopes between −1 and −3 while surface fractals will give slopes between −3 and −4. After 12 h the slope of −2.0 decreases toward −3.0, which indicates that these mass fractal inorganic particulates eventually become more densified colloidal particulates with fractally rough surfaces. The slope of −1.4 most likely

(17) Schaefer, D. W.; Mark, J. E.; McCarthy, D.; Li Jian.; Sun, C.-C.; Bela Farago, *Mater Res. Soc. Symp. Proc.* **1990**, *171*, 57.

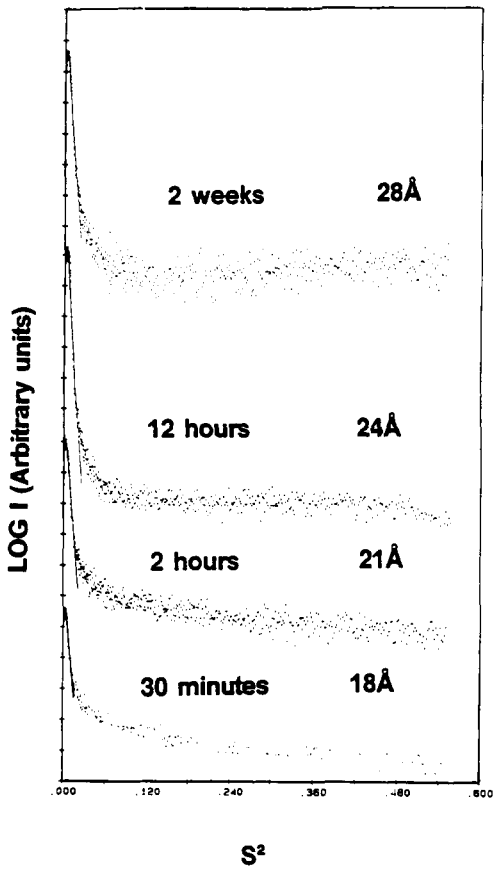

Figure 15. Plot indicates the increase in the radius of gyration with time for the TEOS(60)-PTMO(2K)-100-0.048 ceramer system reacted in DMF/IPA.

arises from a smaller length scale as previously described by Crievich et al. in the study of pure sol gel silicate systems.[18] While we are uncertain of the origin of this "second slope", it is important to recognize that this slope also decreases with time as the reaction progresses until at 2 weeks it becomes indistinguishable from the main slope. These trends suggest that the inorganic particles for this specific ceramer system become more highly densified surface fractals especially when DMF is used as the reacting medium. From the Guinier analysis shown in Figure 15 the radius of gyration also increased with time from 18 Å in 30 min to 28 Å 2 weeks after the addition of the acid catalyst. Hence these results indicate a trend toward the development of more densified particulate structure with eventual surface fractal behavior.

In contrast, the TEOS/PTMO materials reacted in THF/IPA take approximately 6 h to stop flowing (due to a much longer gel time). Upon gelation, the scattering profiles for these films initially do not show any linear regions by which the Porod slope can be estimated. The measured radius of gyration of the scattering particles at this time is around 8 Å. After 2 weeks the scattering profiles did reveal a linear slope in the Porod region of about −1.96 as can be seen in Figure 16. The radius of gyration for these inorganic particles in the ceramer produced in THF/IPA is around 14 Å, 2 weeks after casting. This slope is typical of values obtained on acid catalyzed TEOS by Brinker[10,14] and by several other authors. This fractal dimension indicates that the scattering particles formed in the ceramers reacted in THF/IPA are more linear and ramified as compared with the scattering particulates reacted in DMF/IPA which show surface fractal behavior. The inorganic particulates developed in these ceramers are therefore considered to be mass fractals. Further fractal studies are being conducted on both of these systems as a function of sample composition, and the results will be published at a later date.

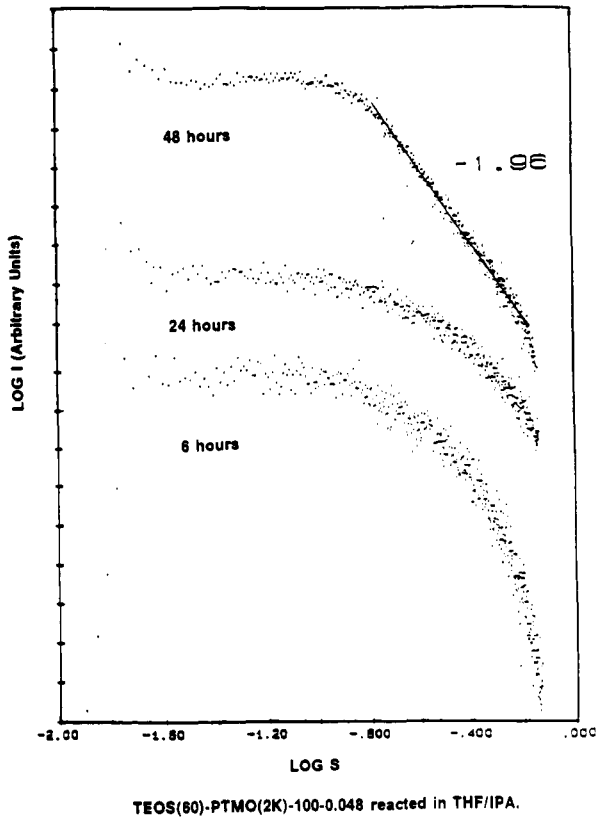

Figure 16. Fractal dimensions obtained (from the Porod region in the SAXS scattering curves) for the TEOS(60)-PTMO(2K)-100-0.048 ceramer reacted in THF/IPA.

Conclusions

From SAXS studies it has been shown that there exists a non-highly periodic fluctuation in electron density within the ceramer systems discussed here due to phase separation between the inorganic and oligomeric components as suggested by the proposed model. The interdomain spacing for these ceramers has been shown to be dependent upon the type and content of metal alkoxide. The model predicts an increase in the interdomain spacing with increasing metal alkoxide content and the SAXS results obtained with increasing TiOPr content confirm this expectation. Since the peak in the scattering profiles were determined to be due to interparticle interference it was seen that by changing the length of the organic matrix spacer between the particles, the interdomain spacing as measured from the SAXS profiles also increases as was expected. Swelling experiments also reveal that an increase in the length of the oligomeric spacer because of solvent uptake causes the interdomain spacing to increase. Finally the scattering intensity has been found to be dependent upon the metal alkoxide content in a given ceramer system as well as the extent of cure within the ceramer system. Thus the morphological model proposed earlier serves as a useful first approximation to account for the expected scattering behavior for these ceramer systems.

The scattering results on the gel prepared in a DMF/IPA medium during formation indicates that with time the inorganic particles develop into highly densified particulates whose surfaces display fractal behavior. The radius

(18) Crievich, A.; dos Santos, D. I.; Aegerter, M.; Lours, T.; Zarzycki, J. *J. Non-Cryst. Solids* 1988, *100*, 424.

of gyration has also been found to increase with time. However, for the same TEOS/PTMO ceramers reacted in THF/IPA, the inorganic particles display more mass fractal behavior. The radius of gyration of the scattering particles also increases with time though the final particle size is much smaller than those developed in the DMF/IPA ceramers.

Acknowledgment. The authors would like to acknowledge the Office of Naval Research for their financial support as well as Don K. Brandom for his assistance with the computational treatement of the SAXS data.

Registry No. TEOS, 78-10-4; $Ti(OPr\text{-}i)_4$, 546-68-9; $Zr(OPr)_4$, 23519-77-9; polytetramethyleneglycol, isocyanatopropyltriethoxysilyl diester, 144126-55-6.

Novel Antimony Sulfides: Synthesis and X-ray Structural Characterization of $Sb_3S_5 \cdot N(C_3H_7)_4$ and $Sb_4S_7 \cdot N_2C_4H_8$

John B. Parise* and Younghee Ko

Department of Earth and Space Sciences, State University of New York, Stony Brook, New York 11794-2100

Received July 28, 1992. Revised Manuscript Received September 27, 1992

Novel antimony sulfides have been synthesized using hydrothermal techniques and organic amines as structure directing agents. The structures of two of these have been solved using single-crystal X-ray diffraction data. One, $Sb_3S_5 \cdot N(C_3H_7)_4$ (SbStpa), forms light yellow blades, has a second harmonic signal 4 times that of quartz, and was synthesized in the presence of tetrapropylammonium hydroxide. The structure contains independent chains of antimony sulfide, infinite in the [100] direction, which are separated by $[N(C_3H_7)]_4^+$ ions. These chains are comprised of edge-linked five-membered rings of SbS_3-pyramids. A second compound, $Sb_4S_7 \cdot N_2C_4H_8$ (SbSpip), crystallizes as red tablets in the presence of triethylenetetramine. The structure incorporates a breakdown product of the added amine, molecules of diprotonated piperazine, $[N_2C_4H_8]^{2+}$. The organic is accommodated between slabs of $[Sb_4S_7]^{2-}$, infinite in the (010) plane. These slabs consist of chains containing three-membered rings of SbS_3-pyramids joined by individual three-coordinated antimony sulfide moieties. Both structures crystallize in the space group *Ama*2 with $a = 10.360$ (2), $b = 23.474$ (3), $c = 9.336$ (1) Å for SbStpa and $a = 9.9498$ (9), $b = 28.513$ (4), and $c = 5.9032$ (8) Å for SbSpip.

Introduction

Recently there has been a growth of interest in novel sulfide structure types.[1-5] This curiosity is sparked by the perceived need to engineer new materials with useful electrical, optical, and ion-exchange properties, or to obtain substances which may be helpful as precursors in the synthesis of such materials.[4] One of the more successful strategies in the *directed* synthesis of oxide materials has recently been applied to sulfides.[1-3] The technique[6] involves the introduction of organic amines into oxide gels or sulfide slurries, followed by hydrothermal crystallization. In the case of oxides, open framework or 2-D structures related to the aluminosilicate zeolites and molecular sieves result.

Using hydrothermal techniques[6-16] adapted for the synthesis of molecular sieves, new open framework materials have been produced from Sb_2S_3.[2,3] In this work, the finely divided sulfide was treated hydrothermally in the presence of alkali metals,[2,6-13] alkali-earth metals,[14] or tertiary amines.[1,3,15,16] These occluded the channels formed about them and were thought to act as structure directing or "templating" agents, during crystallization.[17-19] Further, the black powders recrystallized to produce materials, red[2] to orange[3] in color; this change in color correlated with a decrease in density of the antimony sulfide framework, suggesting an increase in the bandgap.

A natural extension of this work is the use of larger tertiary amines in an attempt to further vary the optical properties and possibly produce materials with larger cavities or with lower structural dimensionality. Reported in this paper are the syntheses of new materials, produced according to this strategy, along with the crystal structures of two of these.

Experimental Section

Synthesis and Characterization. A variety of organic amines (Aldrich Chemical, Table I) have been used in an attempt to direct recrystallization of Sb_2S_3 (Aldrich Chemical). Each potential template was mixed with Sb_2S_3 and H_2O and, in some cases, the amine was reacted with H_2S prior to introduction to the slurries. Addition of H_2S was sometimes found to be efficacious in the

(1) Bedard, R. L.; Wilson, S. T.; Vail, L. D.; Bennett, J. M.; Flanigen, E. M. In *Zeolites: Facts, Figures, Future*; Jacobs, P. A., van Santen, R. A. Eds.; Elsevier Publishing: Amsterdam, 1989.
(2) Parise, J. B. *J. Chem Soc., Chem. Commun.* **1990**, 1553.
(3) Parise, J. B. *Science* **1991**, *251*, 293.
(4) Kanatzidis, M. G. *Comments Inorg. Chem.* **1990**, *10*, 161.
(5) Krebs, B. *Angew. Chem., Int. Ed. Engl.* **1983**, *22*, 113.
(6) Graf, H. A.; Schäfer, H. *Z. Naturforsch.* **1972**, *27b*, 735.
(7) Volf, K.; Schäfer, H. *Z. Naturforsch.* **1978**, *33b*, 827.
(8) Volf, K.; Schäfer, H. *Z. Naturforsch.* **1979**, *34b*, 172.
(9) Eisenmann, B.; Schäfer, H. *Z. Naturforsch.* **1979**, *34b*, 383.
(10) Volf, K.; Schäfer, H. *Z. Naturforsch.* **1979**, *34b*, 1637.
(11) Graf, H. A.; Schäfer, H. *Z. Anorg. Allg. Chem.* **1975**, *414*, 211.
(12) Dittmar, G.; Schäfer, H. *Z. Anorg. Allg. Chem.* **1978**, *441*, 93.
(13) Dittmar, G.; Schäfer, H. *Z. Anorg. Allg. Chem.* **1978**, *441*, 98.
(14) Cordier, G.; Schäfer, H.; Schwidetzky, C. *Z. Naturforsch.* **1984**, *39b*, 131.
(15) Volf, K.; Bickert, P.; Kolmer, R.; Schäfer, H. *Z. Naturforsch.* **1979**, *34b*, 380.
(16) Dittmar, G.; Schäfer, H. *Z. Anorg. Allg. Chem.* **1977**, *437*, 183.
(17) Barrer, R. M. *Hydrothermal Chemistry of the Zeolites*; Academic Press: London, 1982.
(18) Wilson, S. T.; Lok, B. M.; Flanigen, E. M. U.S. Patent 4,310,440, 1982.
(19) Parise, J. B. *J. Chem Soc., Chem. Commun.* **1985**, 606.

0897-4756/92/2804-1446$03.00/0